# Estimation of 3-D Surface Displacement Based on InSAR and Deformation Modeling

Jun Hu, Xiao-Li Ding, Lei Zhang, *Member, IEEE*, Qian Sun, Zhi-Wei Li, Jian-Jun Zhu, and Zhong Lu, *Senior Member, IEEE*

***Abstract*— A new approach is presented for mapping 3-D surface displacement caused by subsurface fluid volumetric change based on 1-D interferometric synthetic aperture radar (InSAR) line-of-sight measurements and surface deformation modeling. The relationship between surface deformation and source fluid volumetric change is modeled according to elastic half-space theory. A distinctive advantage of the proposed approach is that it effectively extends the capability of the sun-synchronous orbit side-looking synthetic aperture radar that has been essentially only able to measure 1-D displacements accurately or at most 2-D displacements when InSAR measurements from more than one orbit or platform are combined. Experimental studies are carried out with both simulated and real data sets to test the performance of the method. The results have demonstrated that the approach works very well.**

***Index Terms*— 3-D displacements, elastic half-space theory, interferometric synthetic aperture radar (InSAR), subsurface fluid.**

## I. Introduction

INTERFEROMETRIC synthetic aperture radar (InSAR) has, in recent decades, become a powerful technique for monitoring surface displacements caused by volumetric changes in underground fluids, such as groundwater, oil, and gas [1]–[4]. Multitemporal InSAR (MT-InSAR) algorithms (e.g., persistent scattererers [5], small baseline subsets [6], and temporarily coherent point [7]) have especially been developed to determine the slow and subtle displacements by better suppressing the inherent InSAR errors, such as decorrelation noises and atmospheric artifacts [4], [8], [9]. However, standard InSAR measurements reflect only the projection of the actual surface displacements onto the line-of-sight (LOS) direction of the radar signals [10], [11]. Since subsurface fluid volumetric change typically causes 3-D surface displacements, the 1-D InSAR LOS measurements are insufficient to provide the required information about the ground deformation and the potential geohazards related to such ground deformation [12].

Complete 3-D displacements can, in theory, be recovered by integrating three or more InSAR LOS measurements with different imaging geometries and covering similar time periods. In fact, the sun-synchronous polar orbit and side-looking imaging geometry of the current SAR can only detect accurately the vertical and east displacements even data from different imaging geometries are used (i.e., the ascending and descending orbits) [11]. In other words, the InSAR LOS measurements are almost "blind" to the north displacement component except at the polar regions [13], [14].

To provide information on the north component of ground surface deformation, offset-tracking [15] and multiaperture InSAR (MAI) [16] techniques have been proposed to provide displacement measurements in the azimuth direction (nearly parallel to the north direction) from InSAR. Complete 3-D displacements can thus be constructed by integrating InSAR-derived LOS measurements and the offset-tracking/MAI derived azimuth measurements with an approach such as weighted least squares (WLSs) algorithm [17]–[22]. Nevertheless, this type of methods is limited only to the investigation of significant displacements (in the order of several centimeters at least) such as those caused by earthquakes, volcano eruptions, and glacier movements due to the limited accuracy of the offset-tracking and MAI techniques. GPS observations can also aid InSAR in resolving reliable 3-D displacements. To integrate InSAR and GPS measurements, the spatially sparse GPS observations need to be interpolated into the same lattice as that of InSAR measurements [23]–[25], or linked to the stress–strain based on the theory of elasticity [26]. Obviously, the method requires a large number of GPS stations, which are not always available.

We will propose a novel approach for inferring 3-D surface displacements caused by subsurface fluid volumetric changes based on 1-D InSAR displacement measurements and elastic half-space theory that exploits the relationship between Earth surface deformation and fluid volumetric changes. A joint model will be constructed that will be able to estimate the 3-D surface displacement and the subsurface fluid volumetric change simultaneously based on the InSAR LOS measurements. A distinctive advantage of the proposed approach is that InSAR LOS measurements of a single track can be used to resolve accurate 3-D displacements. The performance of the proposed approach

Manuscript received May 31, 2016; revised September 29, 2016; accepted November 23, 2016. Date of publication December 26, 2016; date of current version February 24, 2017. This work was supported in part by the National Key Basic Research and Development Program of China under Grant 2013CB733303, in part by the Research Grants Council of the Hong Kong Special Administrative Region under Project PolyU 5147/13E, Project PolyU 5381/13E, Project PolyU 152214/14E, and Project PolyU 152043/14E, in part by the National Natural Science Foundation of China under Grant 41674010, Grant 41404011, Grant 41304011, Grant 41374013, and Grant 41222027, and in part by the Project of Innovation-Driven Plan of Central South University under Grant 2016CX004. *(Corresponding author: Xiao-Li Ding.)*

J. Hu, Z.-W. Li, and J.-J. Zhu are with Central South University, Changsha 410083, China (e-mail: csuhujun@csu.edu.cn; zwli@csu.edu.cn; zjj@csu.edu.cn).

X.-L. Ding and L. Zhang are with The Hong Kong Polytechnic University, Hong Kong (e-mail: lsxlding@polyu.edu.hk; lslzhang@polyu.edu.hk).

Q. Sun is with Hunan Normal University, Changsha 410081, China (e-mail: sunqian200241@aliyun.com).

Z. Lu is with Southern Methodist University, Dallas, TX 75275 USA (e-mail: zhonglu@smu.edu).

Color versions of one or more of the figures in this paper are available online at http://ieeexplore.ieee.org.

Digital Object Identifier 10.1109/TGRS.2016.2634087

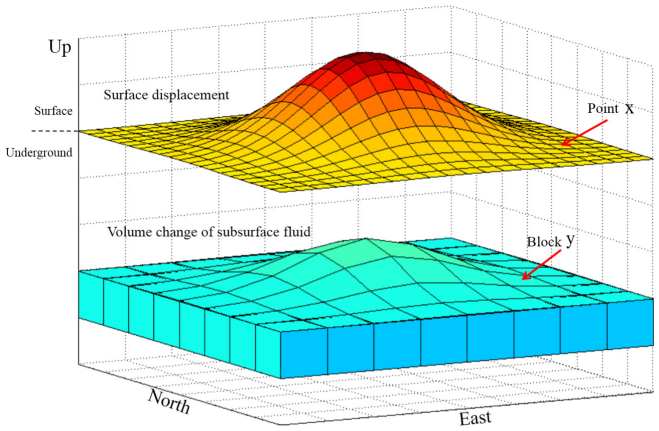


Fig. 1. Surface displacement and volume change of subsurface fluid.

will be verified by experimental studies based on both simulated and real SAR data sets.

## II. Methodology

It is a well-established fact that underground fluid flow can lead to ground deformation [27], [28]. To understand subsurface fluid status, great efforts have been made to model subsurface fluid volumetric change based on ground deformation observed by geodetic techniques, such as leveling, GPS, and InSAR [1], [28]–[34]. In this process, an assumption commonly made is that the source volume lies within a homogeneous half-space and the Earth deforms elastically [35], [36]. This is obviously an idealization, but is applicable in investigating most subsurface fluid changes even when the surrounding earth medium is heterogeneous due to layering and faults [36]. According to the elastic half-space theory, the relationship between the surface displacement and the volumetric change of the subsurface fluids is [37]

$$d_l(x) = \int_V G_l(x, y) D_v(y) dy \tag{1}$$

where $d_l(x)$ represents the surface displacement at point $x$, with $l = 1, 2, 3$ indicating the east, north, and up components, respectively; $D_v(y)$ represents the fractional fluid volumetric change of a block at point $y$ within a source volume $V$; $G_l(x, y)$ is Green's function defined as

$$G_l(x, y) = \frac{(v+1)}{3\pi} \frac{(x_l - y_l)}{S^3} \tag{2}$$

where $v$ is Poisson's ratio; $S = ((x_1 - y_1)^2 + (x_2 - y_2)^2 + (x_3 - y_3)^2)^{1/2}$ is the distance between block $y$ and point $x$ [30], [38].

Fig. 1 shows the concept presented in (1). The surface displacement at each point (e.g., $x_i$) is the accumulative contribution of all the blocks within the underground source volume. We assume that the underground source volume can be discretized into $N$ blocks. Considering that $M$ observation points are provided by the InSAR LOS measurements, the 3-D surface displacement of point $x_i, (i = 1, 2, \cdots, M)$ due to subsurface fluid volumetric change can be written as

$$\begin{bmatrix} d_1(x_i) \\ d_2(x_i) \\ d_3(x_i) \end{bmatrix} = \begin{bmatrix} V_y \times G_1(x_i, y_1) & V_y \times G_1(x_i, y_2) \cdots V_y \times G_1(x_i, y_N) \\ V_y \times G_2(x_i, y_1) & V_y \times G_2(x_i, y_2) \cdots V_y \times G_2(x_i, y_N) \\ V_y \times G_3(x_i, y_1) & V_y \times G_3(x_i, y_2) \cdots V_y \times G_3(x_i, y_N) \end{bmatrix} \cdot \begin{bmatrix} D_v(y_1) \\ D_v(y_2) \\ \vdots \\ D_v(y_N) \end{bmatrix} - \begin{bmatrix} \varepsilon_1(x_i) \\ \varepsilon_2(x_i) \\ \varepsilon_3(x_i) \end{bmatrix} \tag{3}$$

where $V_y$ is the volume of block $y_j (j = 1, 2, \cdots, N)$. $\varepsilon_l(x_i)$ represents the model error of (1) at point $x_i$, which could be induced by such factors as existence of a fault within the source volume [36].

Assuming that InSAR LOS displacement measurement at point $x_i$ is acquired by using data from a single orbit track, the InSAR LOS measurement $I(x_i)$ can be written as [10]

$$I(x_i) = [\, S_1(x_i) \quad S_2(x_i) \quad S_3(x_i) \,] \cdot [\, d_1(x_i) \quad d_2(x_i) \quad d_3(x_i) \,]^T + \eta(x_i) \tag{4}$$

where $\eta(x_i)$ is the InSAR observation errors at point $x_i$, due to, e.g., decorrelation noise, residual topographic error, atmospheric artifact, and orbital error; $S_1(x_i)$, $S_2(x_i)$, and $S_3(x_i)$ represent the projection coefficients of InSAR LOS measurement at point $x_i$ for east, north, and up directions, respectively

$$\begin{cases} S_1(x_i) = -\cos\alpha_i \cdot \sin\theta_i \\ S_2(x_i) = \sin\alpha_i \cdot \sin\theta_i \\ S_3(x_i) = \cos\theta_i \end{cases} \tag{5}$$

where $\theta_i$ and $\alpha_i$ are the radar incidence angle and azimuth angle (clockwise from the north) of point $x_i$, respectively.

Equations (3) and (4) can be combined to form a joint model that involves all the observed points and underground volume blocks

$$\Omega = B\Gamma + \Delta \tag{6}$$

where $\Omega$ is the $4M \times 1$ observation matrix

$$\Omega_{4M\times 1} = [I(x_1) \ \cdots \ I(x_M) \ 0 \ 0 \ 0 \ \cdots \ \cdots \ \cdots \ 0 \ 0 \ 0]^T$$

$\Delta$ is the $4M \times 1$ residual matrix

$$\Delta_{4M\times 1} = [\eta(x_1) \ \cdots \ \eta(x_M) \ \varepsilon_1(x_1) \ \varepsilon_2(x_1) \ \varepsilon_3(x_1) \ \cdots \ \cdots \ \cdots \ \varepsilon_1(x_M) \ \varepsilon_2(x_M) \ \varepsilon_3(x_M)]^T$$

$\Gamma$ is the $(3M + N) \times 1$ vector of unknown parameters, constituting of the 3-D surface displacements of the $M$ points and the fractional volumetric changes of the $N$ blocks

$$\Gamma_{(3M+N)\times 1} = [d_1(x_1) \ d_2(x_1) \ d_3(x_1) \ \cdots \ \cdots \ \cdots \ d_1(x_M) \ d_2(x_M) \ d_3(x_M) \ D_v(y_1) \ \cdots \ D_v(y_N)]^T$$

and $B$ is the $4M \times (3M + N)$ design matrix, as shown at the bottom of the page.

When the number of observed points $M$ is larger than the number of blocks $N$, the joint model in (6) can be resolved by

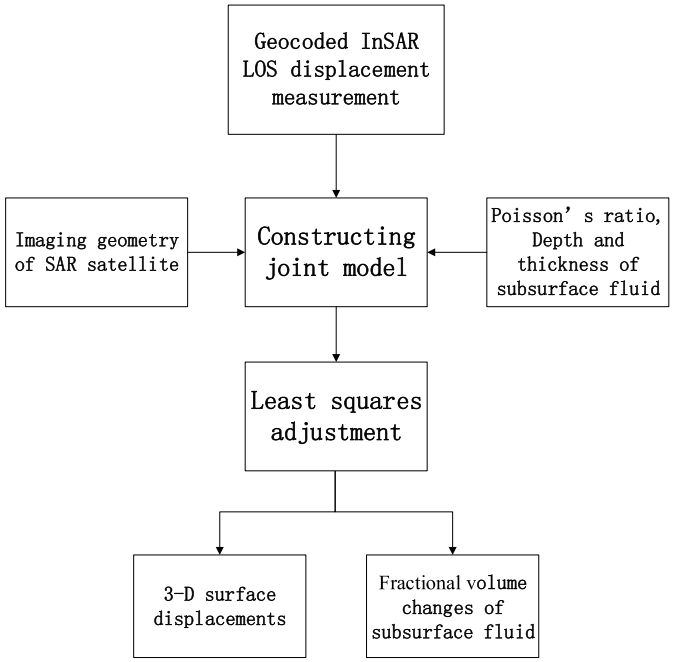


Fig. 2. Block diagram of the approach.

applying least squares principle. This is usually a large sparse linear system, and the unknown parameters can be estimated by using an iterative method based on, e.g., the Golub and Kahan bidiagonalization procedure [39], [40].

The joint model in (6) can accommodate InSAR LOS measurements from different orbit tracks, and thus the redundancy of the equation system can be increased to $t \times M - N$ ($t$ is the number of orbit tracks). In addition, the underground source volume can be more than one layer when necessary. A block diagram illustrating the main steps of the approach is shown in Fig. 2.

Although (6) is overdetermined, the system might be unstable due to its possible ill-condition [35]. In order to stabilize the least-squares inversion, a roughness penalty can be included in the joint model. A matrix that estimates the spatial derivative of the fractional volume change can be added as the penalty matrix, with a weighting factor to control the level of the roughness. Such a term can characterize a connected network of subsurface fluids rather than isolated blocks [34], [35].

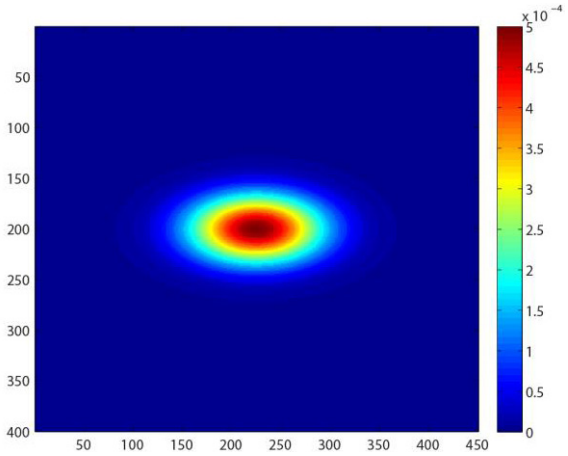


Fig. 3. Simulated fractional volume changes of subsurface fluid.

## III. Experiments With Simulated Data

The performance of the approach is first evaluated by using a series of simulation experiments. As shown in Fig. 3, the fractional volumetric change of the subsurface fluid is simulated over a $400 \times 450$ grid based on

$$D_v(i, j) = D_{v,\max} \cdot e^{-((i^2+j^2)/\omega)} \tag{7}$$

where $D_v(i, j)$ is the fractional volumetric change at a block $(i, j)$; $D_{v,\max}$ is the maximum value of the fractional volumetric change ($D_{v,\max} = 5 \times 10^{-4}$ in this simulation); and $\omega$ is the term that controls the gradient and the size of the volumetric changes. The grid sizes are all 10 m $\times$ 10 m. The depth and thickness of the simulated subsurface fluid are both 100 m. A typical Poisson's ratio of 0.25 is used in this paper.

According to (1), 3-D surface displacements are calculated from the simulated fractional fluid volumetric change [see Fig. 4(a)–(c)]. InSAR LOS measurements from ascending

$$B_{4M\times(3M+N)} = \begin{bmatrix}
S_1(x_1) & S_2(x_1) & S_3(x_1) & 0 & 0 & 0 & \cdots & 0 & 0 & 0 & 0 & 0 & \cdots & 0 \\
0 & 0 & 0 & S_1(x_2) & S_2(x_2) & S_3(x_2) & \vdots & \vdots & \vdots & \vdots & 0 & 0 & \cdots & 0 \\
\vdots & \vdots & \vdots & \cdots & \cdots & \cdots & \ddots & 0 & 0 & 0 & \vdots & \vdots & \vdots & \vdots \\
0 & 0 & 0 & 0 & 0 & 0 & \cdots & S_1(x_M) & S_2(x_M) & S_3(x_M) & 0 & 0 & \cdots & 0 \\
1 & 0 & 0 & 0 & 0 & 0 & \cdots & 0 & 0 & 0 & -V_yG_1(x_1,y_1) & -V_yG_1(x_1,y_2) & \cdots & -V_yG_1(x_1,y_N) \\
0 & 1 & 0 & 0 & 0 & 0 & \cdots & 0 & 0 & 0 & -V_yG_2(x_1,y_1) & -V_yG_2(x_1,y_2) & \cdots & -V_yG_2(x_1,y_N) \\
0 & 0 & 1 & 0 & 0 & 0 & \cdots & 0 & 0 & 0 & -V_yG_3(x_1,y_1) & -V_yG_3(x_1,y_2) & \cdots & -V_yG_3(x_1,y_N) \\
0 & 0 & 0 & 1 & 0 & 0 & \cdots & 0 & 0 & 0 & -V_yG_1(x_2,y_1) & -V_yG_1(x_2,y_2) & \cdots & -V_yG_1(x_2,y_N) \\
0 & 0 & 0 & 0 & 1 & 0 & \cdots & 0 & 0 & 0 & -V_yG_2(x_2,y_1) & -V_yG_2(x_2,y_2) & \cdots & -V_yG_2(x_2,y_N) \\
0 & 0 & 0 & 0 & 0 & 1 & \vdots & 0 & 0 & 0 & -V_yG_3(x_2,y_1) & -V_yG_3(x_2,y_2) & \cdots & -V_yG_3(x_2,y_N) \\
\vdots & \vdots & \vdots & \vdots & \vdots & \vdots & \ddots & \vdots & \vdots & \vdots & \vdots & \vdots & \vdots & \vdots \\
0 & 0 & 0 & 0 & 0 & 0 & \cdots & 1 & 0 & 0 & -V_yG_1(x_M,y_1) & -V_yG_1(x_M,y_2) & \cdots & -V_yG_1(x_M,y_N) \\
0 & 0 & 0 & 0 & 0 & 0 & \cdots & 0 & 1 & 0 & -V_yG_2(x_M,y_1) & -V_yG_2(x_M,y_2) & \cdots & -V_yG_2(x_M,y_N) \\
0 & 0 & 0 & 0 & 0 & 0 & \cdots & 0 & 0 & 1 & -V_yG_3(x_M,y_1) & -V_yG_3(x_M,y_2) & \cdots & -V_yG_3(x_M,y_N)
\end{bmatrix}$$

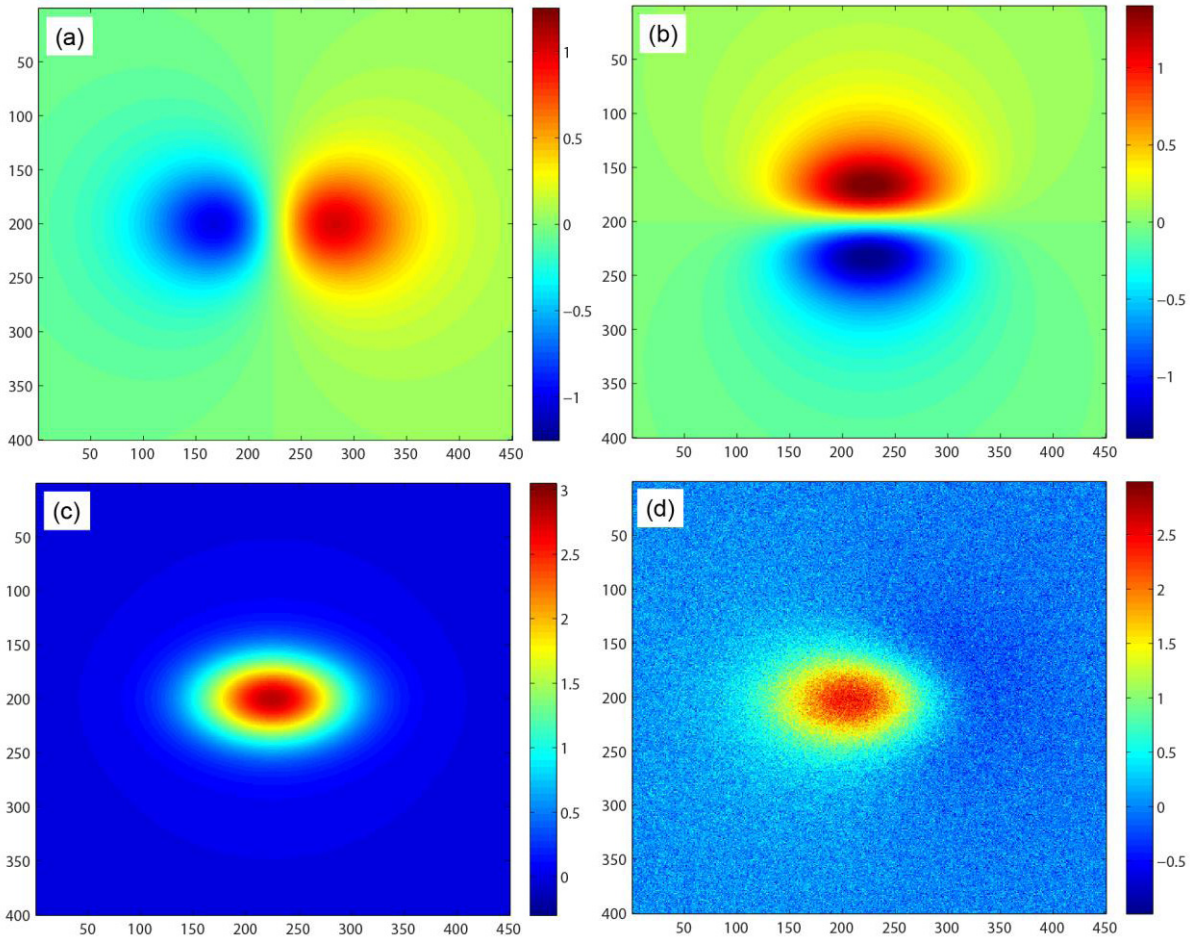


Fig. 4. Surface displacements induced by the simulated fractional volume change of the subsurface fluid. (a) East component. (b) North component. (c) Up component. (d) LOS component with simulated noises (unit: cm).

TABLE I

RMSEs OF ESTIMATED 3-D SURFACE DISPLACEMENT FROM THE INSAR LOS MEASUREMENTS WITH DIFFERENT LEVELS OF NOISE

| STDs of InSAR observation noise (mm) | RMSEs of the 3-D displacement estimations | | |
|---|---|---|---|
| | East (mm) | North (mm) | Up (mm) |
| 0 | 0.1 | 0.2 | 0.1 |
| 1 | 0.3 | 0.2 | 0.4 |
| 2 | 0.6 | 0.2 | 0.8 |
| 5 | 1.6 | 0.5 | 2.0 |
| 10 | 3.1 | 1.1 | 4.1 |
| 20 | 6.3 | 2.0 | 8.1 |

orbit track are then simulated over a 400 × 450 grid by using (4), where the SAR radar system parameters are the same as the advanced land observing satellite (ALOS) phased array-type $L$-band SAR (PALSAR) data over the Kilauea volcano, Hawaii, which will also be used in Section IV. For simplification, a zero-mean additive Gaussian noise with 2-mm standard deviation (STD) is added to the InSAR measurements as the InSAR observation noise [see Fig. 4(d)].

The 3-D surface displacements and the fractional fluid volumetric change are estimated from the simulated InSAR LOS measurements based on (6). To enhance the redundancy of the equation system, the fluid volumetric change is estimated over a $40 \times 45$ grid rather than over the original $400 \times 450$ grid. The coarser resolution is sufficient in describing the variation of the subsurface fluid although some approximation errors due to the downsampling operation may be introduced [35], [36].

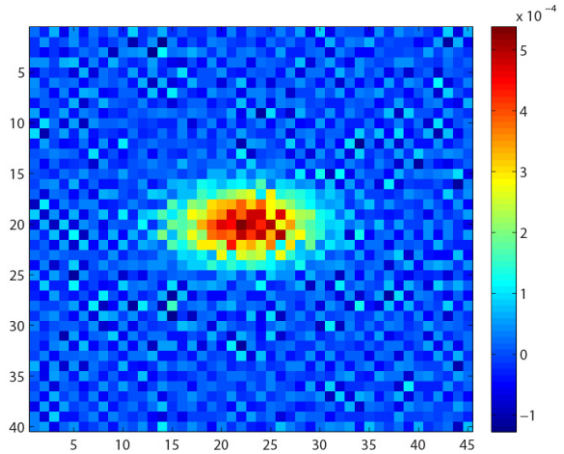

Fig. 5. Estimated fractional volume changes from the joint model.

Fig. 5 shows the estimated fractional fluid volumetric change that has clearly a similar pattern to the simulated volumetric change, although the spatial resolution is 100 times lower. Fig. 6(a)–(c) shows the 3-D surface displacement maps estimated from the joint model. It is found that

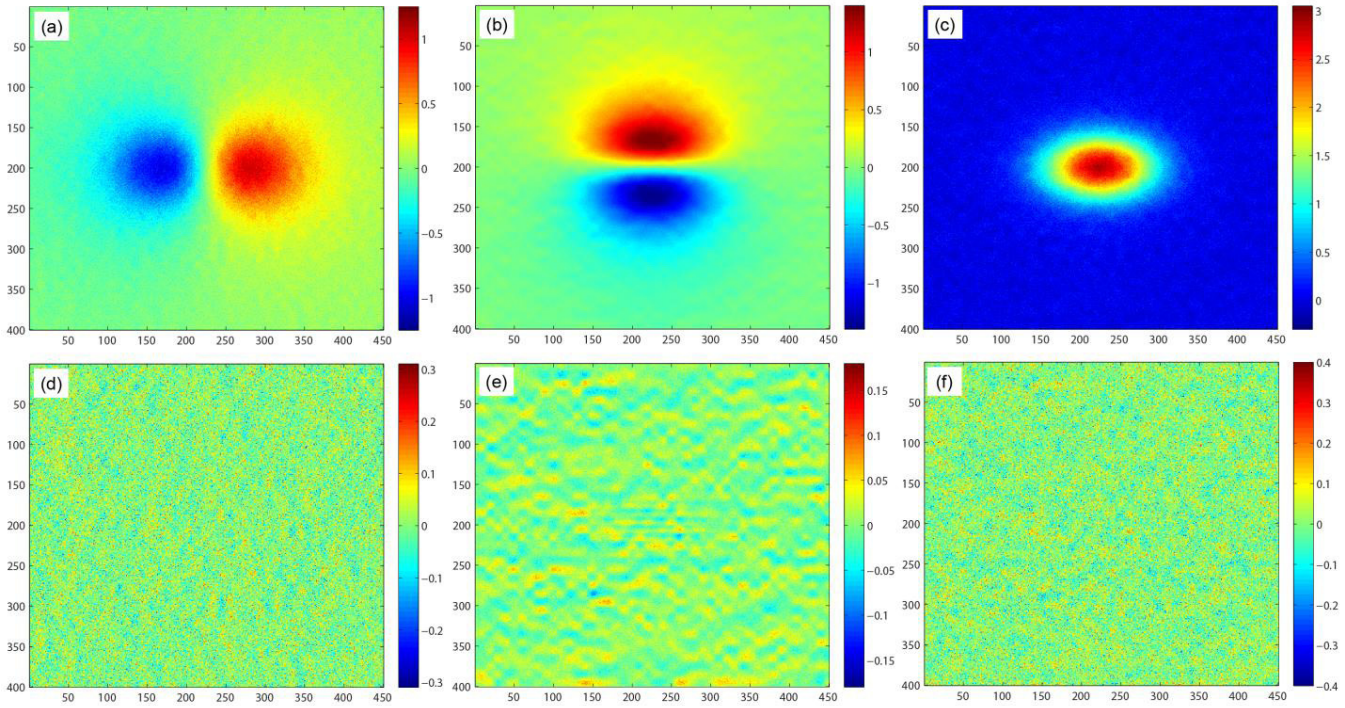


Fig. 6. (a)–(c) Estimated 3-D surface displacements from the joint model. (d)–(f) Differences between the estimated and simulated 3-D surface displacements. (Left) East component. (Middle) North component. (Right) Up component (unit: cm).

TABLE II
BASIC INFORMATION OF THE USED ALOS PALSAR DATA

| No. | Orbit | Path | Frame | Master | Slave | Perpendicular baselines (m) | Time interval (days) |
|---|---|---|---|---|---|---|---|
| 1 | Ascending | 291 | 370 | May 5, 2007 | Jun. 20, 2007 | -325 | 46 |
| 2 | Descending | 601 | 3230 | Feb. 28, 2007 | Jul. 16, 2007 | 250 | 138 |

the three components appear all agree well with the simulated ones. Fig. 6(d)–(f) gives the differences between the estimated and the simulated 3-D surface displacements. It seems that the differences in the east and up directions are dominated by Gaussian noise. This is expected, since the simulated errors added to the InSAR LOS measurements are propagated mostly into these two components due to the relative larger projection coefficients in the east and up directions (i.e., about 0.6 and 0.7, respectively). The grid pattern in the north direction is considered due to downsampling of the grid of the estimated fractional fluid volumetric change.

The root-mean-square errors (RMSEs) of the differences between the simulated and the estimated 3-D surface displacement values are calculated to provide a quantitative assessment of the performance of the proposed approach. Different levels of noise (0, 1, 2, 5, 10, and 20 mm in STDs) are added to the InSAR LOS measurements in the experiment. As shown in Table I, the RMSEs increase with the STDs of the InSAR LOS measurements, but the RMSEs of the estimated deformation are smaller than the STDs of the InSAR observations. Even when the InSAR observation errors increase to 20 mm, the STDs of the estimated deformation components are still within 10 mm. This indicates that the joint model can efficiently suppress the effect of InSAR observation noise. The north component is most accurate when observation noise is added. However, the RMSE of the north component is twice of those of the other two components when no noise is added to the InSAR LOS measurements. This also demonstrates that the north displacement estimations depend mainly on the joint model.

## IV. EXPERIMENTS WITH REAL DATA

As one of the five active shield volcanos on Hawaii Islands, Kilauea volcano has fitfully erupted since January 3, 1983 [41]. On June 17, 2007, a new episode of eruptions occurred with rapid deflation at the summit [42]. The volcanic activities were recorded by many geodetic techniques, such as tilt meters, GPS, and InSAR, among which Jung *et al.* [19] had mapped the complete 3-D displacement fields by employing two InSAR-derived LOS measurements and two MAI-derived azimuth measurements provided by the cross-heading ALOS PALSAR tracks (see Table II). The surface deformation of a volcano is often related to volcanic and tectonic sources, and is difficult to be described by a simple fluid volumetric model. In this paper, we only focus on the deformation of the caldera of Kilauea volcano, which should mainly be caused by the intrusion and eruption of the magma [45] and can be modeled more easily. We use the proposed approach to estimate the complete 3-D displacements of the Kilauea caldera from only the InSAR LOS measurements provided by ALOS PALSAR ascending orbit (i.e., the first pair in Table II). The shaded relief map of the study region is shown as Fig. 7(a),

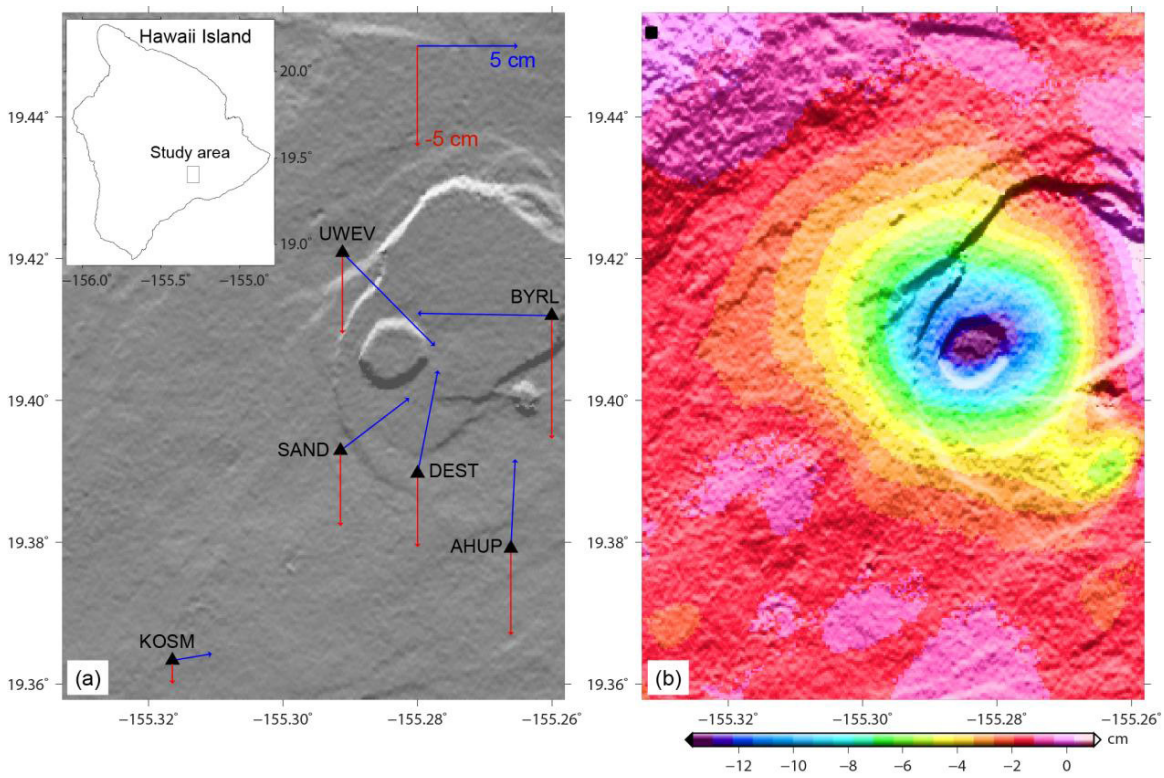


Fig. 7. (a) Shaded relief map of Kilauea caldera. Triangles represent the locations of GPS sites. The red and blue arrows represent the vertical and horizontal components of the GPS displacement observations, respectively. The inset map shows the location of the study area in the Hawaii Island. (b) Displacement in the LOS direction derived from the ALOS PALSAR ascending interferogram. Square represents the reference area.

which is generated from 1-arcsec shuttle radar topography mission (SRTM) data. Note that the descending PALSAR pair (i.e., the second pair in Table II) is not used in the joint model to avoid the decorrelation noise caused by its relative longer time interval. Furthermore, the volcanic activities during the investigated period may induce different ground movements to the ascending and descending pairs that have different temporal spans.

With the PALSAR images acquired on May 5 and June 20, 2007, a differential interferogram with a time interval of 46 days and perpendicular baseline of 325 m is generated using a two-pass Differential Interferometric Synthetic Aperture Radar approach. Multilook operation (i.e., 3 looks in range and 14 looks in azimuth directions) is carried out to reduce the noise in the data. The contribution of topographic phase is simulated and removed by using the 1-arcsec SRTM Digital Elevation Model (DEM) [Fig. 7(a)]. Before the retrieval of the phase integer ambiguities with the minimum cost flow algorithm [43], we apply a least-squares-based filter [44] to the differential interferogram to further suppress the effects of the noise. Bi-quadratic and linear polynomial models are applied to the unwrapped differential interferogram to reduce the effects of the potential orbit errors and stratified atmospheric artifacts. Finally, the displacement measurements along the PALSAR ascending LOS direction are converted from the differential interferogram via a multiplication of $\lambda/4\pi$ (where $\lambda$ is radar wavelength), and then transformed into the World Geodetic System 1984 coordinate system, resulting in a spatial resolution of about 30 m $\times$ 30 m. The LOS displacement field of the Kilauea caldera is shown in Fig. 7(b), where the black square represents the reference area used in the InSAR data processing.

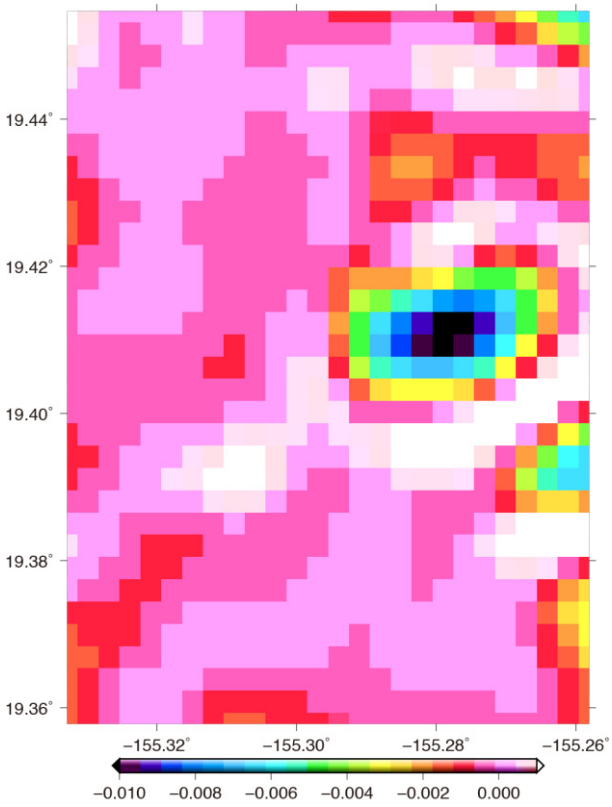


Fig. 8. Estimated fractional volume changes of the magma beneath the Kilauea caldera.

Besides the geocoded InSAR LOS displacement measurements, the SAR imaging geometry and some *a priori* knowledge about the magma should be provided when

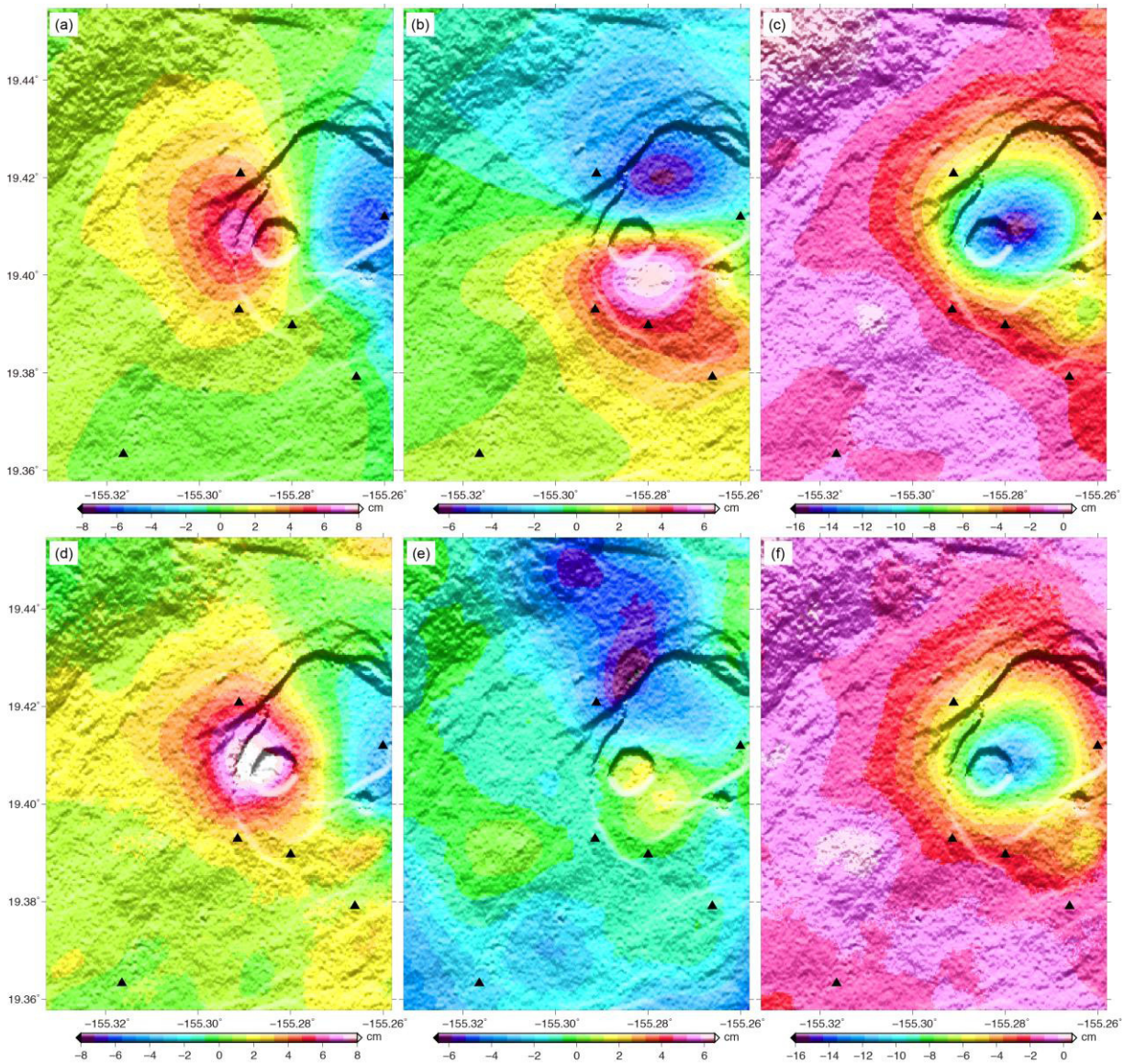


Fig. 9. Estimated 3-D surface displacements of the Kilauea caldera from (a)–(c) joint model and (d)–(f) WLS method. Triangles represent the locations of the GPS sites. (Left) East component. (Middle) North component. (Right) Up component.

TABLE III

DIFFERENCES BETWEEN THE ESTIMATED 3-D SURFACE DISPLACEMENTS FROM INSAR AND GPS OBSERVATIONS

| GPS sites | Differences in east (mm) | | Differences in north (mm) | | Differences in up (mm) | |
|---|---|---|---|---|---|---|
| | Joint model | WLS method | Joint model | WLS method | Joint model | WLS method |
| AHUP | 2.4 | -12.6 | 16.5 | 55.1 | -21.8 | -26.2 |
| BYRL | -8.5 | -32.6 | 11.2 | 11.2 | -7.9 | -26.6 |
| KOSM | 14.9 | 15.1 | -5.9 | 24.5 | 0.7 | 6.2 |
| UWEV | 8.0 | -0.8 | -10.6 | -4.4 | 12.9 | 6.6 |
| SAND | 5.6 | 6.3 | -8.9 | 35.3 | -13.5 | -8.0 |
| DEST | -3.3 | -12.2 | 8.7 | 55.9 | -8.8 | -10.1 |
| **RMSEs** | **8.2** | **16.5** | **10.8** | **36.9** | **12.7** | **16.6** |

applying the joint model. We estimate the local incidence angle and azimuth angle for each pixel from the PALSAR sensor's parameters and the local topography provided by SRTM DEM. Poisson's ratio of 0.25 is assumed [45]. Following [46], the depth of the magma is assumed to be 1.25 km. It is quite difficult to determine the value of thickness of the magma in reality. We use a typical thickness of 100 m and assume that the volumetric change occurs predominantly in the uppermost layer of the magma. In addition, we downsample the fractional magma volumetric change to a spatial resolution of about 300 m $\times$ 300 m, which is 100 times low in resolution than the surface displacements. A roughness penalty is included

in the inversion of Kilauea caldera to avoid the instability probably due to the great depth of the magma. We select 10 as the weight of the roughness penalty term, based on the examination of the misfit between the InSAR-derived and the reestimated LOS deformations.

Fig. 8 shows the estimated fractional magna volumetric change beneath the Kilauea caldera during May 5 and June 20, 2007 from the proposed approach. It is seen that the most evident activities occurred in and around the caldera. It is determined that the magma changed its volume by $-4.6 \times 10^6$ m$^3$ during this time period. The results provide a reasonable physical evidence that is related to volcano sources. The 3-D displacement maps estimated are shown in Fig. 9(a)–(c). As expected, the ground subsided and moved toward central area of the caldera as a result of the reduction of the subsurface magna volume and the deflation of the surface area. The maximum vertical displacement reached $-16$ cm, at the center of the caldera. While the east and north displacements are roughly symmetrical with respect to the center of the caldera, in the range of $-6$–6 cm. Benefited from the good quality of the used InSAR LOS measurements, all the three displacement components from the solution look very clear and smooth, indicating fairly low level of noise in the results.

For comparison, the 3-D displacements of the Kilauea caldera have also been estimated by applying a WLSs adjustment model based on the InSAR and MAI measurements from the ascending and descending pairs listed in Table II. In the MAI processing, a half normalized squint is adopted in the azimuth common band filtering to generate the backward- and forward-looking SAR images. Besides, we use the method proposed in [47] to eliminate the phase residuals induced by minor difference between the perpendicular baselines of the backward- and forward-looking interferograms. The weights of the InSAR or MAI observations are determined according to the STDs that are calculated with a $5 \times 5$ window sliding over the observations [19], [21]. Fig. 9(d)–(f) shows the 3-D displacement maps estimated from the WLS-based method. In general, the three deformation components are similar to those estimated from the joint model proposed in this paper, especially the up component. However, the ground subsidence at the caldera derived from WLS-based method are somewhat smaller than that from the new method. Since the caldera switched from deflation to inflation from June 19, 2007 [42], some subsidence were neutralized by the subsequent uplift in the PALSAR descending measurement that covers a longer period. This can explain the difference between the joint model and the WLS-based results. It is also found that the north displacement field derived from WLS-based method is contaminated by bubble-shaped deformations, which are not expected in this area. This could be ascribed to the errors in the MAI measurements, which dominate the north component but are not accurate enough to estimate centimeter-level surface displacements.

The activity of the Kilauea caldera was also recorded by six GPS sites (AHUP, BYRL, KOSM, UWEW, SAND, and DEST), which are employed in this paper to cross validate the InSAR results. The locations of the GPS sites are shown as triangles in Figs. 7(a) and 9. A $3 \times 3$ pixel window over each of the GPS sites is used to calculate the average displacement from the InSAR results for comparison with the GPS results. The differences between the 3-D displacements estimated from the joint model and WLS-based approaches and the GPS 3-D displacement observations at the six sites are provided in Table III. We can clearly observe that the new approach in general offers better accuracy than the WLS-based approach for all the three components. The RMSEs of the results from the joint model are 8.2, 10.8, and 12.7 mm for the east, north, and up components, respectively, while those of the results from the WLS-based model are 16.5, 36.9, and 16.6 mm, respectively. Improvements of 50.3%, 70.7%, and 23.5% have been achieved for the east, north, and up components, respectively. The greatest improvement in the north direction demonstrates that the new approach is more suitable for monitoring 3-D surface displacements associated with subsurface fluid changes than the purely InSAR-based approaches. The relatively larger RMSE errors of the up results may be partly due to the inferior vertical positioning accuracy of GPS.

## V. Conclusion

Knowledge on complete and spatially continuous 3-D surface displacements is of great importance for studying the surface deformation and associated geohazards due to subsurface fluid volumetric change. A new method is proposed in this paper to derive 3-D surface displacement and subsurface fluid change based on InSAR LOS measurements and deformation modeling according to elastic half-space theory. Experiments with both simulated and real data sets have shown that the new method can accurately estimate 3-D displacements associated with subsurface fluid changes. The results are more accurate than those from pure InSAR measurements. The proposed approach should be useful for studying various phenomena such as subsidence due to water and oil extraction.

Further work can be done to improve the proposed method. First, the joint model needs some *a priori* knowledge about the site, e.g., Poisson's ratio of the earth material, and the depth and thickness of the fluid volume. When such knowledge is unavailable, an iterative approach may be developed to estimate such information as part of the inversion process. Second, the single layer assumption and the coarse spatial resolution of the fluid blocks may be insufficient in certain applications. Third, the joint model can be integrated with multisensor, multitrack, and multitemporal InSAR measurements based on a Kalman filter approach [48] to improve the temporal resolution of the solution.

## Acknowledgment

The authors would like to thank the two anonymous reviewers for their constructive comments and suggestions. The ALOS PALSAR data were provided by the Japan Aerospace Exploration Agency.

## References

[1] C. Wicks, Jr., W. Thatcher, and D. Dzurisin, "Migration of fluids beneath Yellowstone Caldera inferred from satellite radar interferometry," *Science*, vol. 282, no. 5388, pp. 458–462, Oct. 1998.

[2] Y. Fialko and M. Simons, "Deformation and seismicity in the Coso geothermal area, Inyo County, California: Observations and modeling using satellite radar interferometry," *J. Geophys. Res.*, vol. 105, no. B9, pp. 21781–21793, Sep. 2000.

[3] G. W. Bawden, W. Thatcher, R. S. Stein, K. W. Hudnut, and G. Peltzer, "Tectonic contraction across Los Angeles after removal of groundwater pumping effects," *Nature*, vol. 412, no. 6849, pp. 812–815, Aug. 2001.

[4] D. W. Vasco *et al.*, "Satellite-based measurements of surface deformation reveal fluid flow associated with the geological storage of carbon dioxide," *Geophys. Res. Lett.*, vol. 37, no. 3, pp. L03303-1–L03303-5, Feb. 2010.

[5] A. Ferretti, C. Prati, and F. Rocca, "Nonlinear subsidence rate estimation using permanent scatterers in differential SAR interferometry," *IEEE Trans. Geosci. Remote Sens.*, vol. 38, no. 5, pp. 2202–2212, Sep. 2000.

[6] P. Berardino, G. Fornaro, R. Lanari, and E. Sansosti, "A new algorithm for surface deformation monitoring based on small baseline differential SAR interferograms," *IEEE Trans. Geosci. Remote Sens.*, vol. 40, no. 11, pp. 2375–2383, Nov. 2002.

[7] L. Zhang, X. L. Ding, and Z. Lu, "Modeling PSInSAR time series without phase unwrapping," *IEEE Trans. Geosci. Remote Sens.*, vol. 49, no. 1, pp. 547–556, Jan. 2011.

[8] R. Lanari, P. Lundgren, M. Manzo, and F. Casu, "Satellite radar interferometry time series analysis of surface deformation for Los Angeles, California," *Geophys. Res. Lett.*, vol. 31, no. 23, pp. L23613-1–L23613-5, Dec. 2004.

[9] L. Zhang, Z. Lu, X. L. Ding, H. S. Jung, G. C. Feng, and C. W. Lee, "Mapping ground surface deformation using temporarily coherent point SAR interferometry: Application to Los Angeles Basin," *Remote Sens. Environ.*, vol. 117, pp. 429–439, Feb. 2012.

[10] T. J. Wright, B. E. Parsons, and Z. Lu, "Toward mapping surface deformation in three dimensions using InSAR," *Geophys. Res. Lett.*, vol. 31, no. 1, pp. L01607-1–L01607-5, Jan. 2004.

[11] J. Hu, Z. W. Li, X. L. Ding, J. J. Zhu, L. Zhang, and Q. Sun, "Resolving three-dimensional surface displacements from InSAR measurements: A review," *Earth-Sci. Rev.*, vol. 133, pp. 1–17, Jun. 2014.

[12] S. Samieie-Esfahany, R. F. Hanssen, K. V. Thienen-Visser, and A. Muntendam-Bos, "On the effect of horizontal deformation on InSAR subsidence estimates," in *Proc. Fringe Workshop*, 2009, pp. 1–7.

[13] L. Gray, "Using multiple RADARSAT InSAR pairs to estimate a full three-dimensional solution for glacial ice movement," *Geophys. Res. Lett.*, vol. 38, no. 5, pp. L05502-1–L05502-6, Mar. 2011.

[14] M. Manzo *et al.*, "Surface deformation analysis in the Ischia Island (Italy) based on spaceborne radar interferometry," *J. Volcanol. Geothermal Res.*, vol. 151, no. 4, pp. 399–416, Mar. 2006.

[15] R. Michel, J. Taboury, and J. Avouac, "Measuring ground displacements from SAR amplitude images: Application to the Landers earthquake," *Geophys. Res. Lett.*, vol. 26, no. 7, pp. 875–878, Apr. 1999.

[16] N. B. D. Bechor and H. A. Zebker, "Measuring two-dimensional movements using a single InSAR pair," *Geophys. Res. Lett.*, vol. 33, no. 16, pp. L16311-1–L16311-5, Aug. 2006.

[17] Y. Fialko, M. Simons, and D. Agnew, "The complete (3-D) surface displacement field in the epicentral area of the 1999 $M_W$ 7.1 Hector Mine earthquake, California, from space geodetic observations," *Geophys. Res. Lett.*, vol. 28, no. 16, pp. 3063–3066, Aug. 2001.

[18] Y. Fialko, D. Sandwell, M. Simons, and P. Rosen, "Three-dimensional deformation caused by the Bam, Iran, earthquake and the origin of shallow slip deficit," *Nature*, vol. 435, no. 7040, pp. 295–299, May 2005.

[19] H. Jung, Z. Lu, J. Won, M. Poland, and A. Miklius, "Mapping three-dimensional surface deformation by combining multiple-aperture interferometry and conventional interferometry: Application to the June 2007 eruption of Kilauea Volcano, Hawaii," *IEEE Geosci. Remote Sens. Lett.*, vol. 8, no. 1, pp. 34–38, Jan. 2010.

[20] N. Gourmelen *et al.*, "Ice velocity determined using conventional and multiple-aperture InSAR," *Earth Planetary Sci. Lett.*, vol. 307, nos. 1–2, pp. 156–160, Jul. 2011.

[21] J. Hu, Z. W. Li, X. L. Ding, J. J. Zhu, L. Zhang, and Q. Sun, "3D coseismic displacement of 2010 Darfield, New Zealand earthquake estimated from multi-aperture InSAR and D-InSAR measurements," *J. Geodesy*, vol. 86, no. 11, pp. 1029–1041, Nov. 2012.

[22] M. J. Jo, H. S. Jung, J. S. Won, and P. Lundgren, "X-band radar interferometry: Application to the March 2011 Kamoamoa fissure eruption, Kilauea Volcano, Hawai'i," *Remote Sens. Environ.*, vol. 169, pp. 176–191, Nov. 2015.

[23] S. Gudmundsson, F. Sigmundsson, and J. Carstensen, "Three-dimensional surface motion maps estimated from combined interferometric synthetic aperture radar and GPS data," *J. Geophys. Res.*, vol. 107, no. B10, pp. 2250–2264, 2002.

[24] S. Samsonov, K. Tiampo, J. Rundle, and Z. H. Li, "Application of DInSAR-GPS optimization for derivation of fine-scale surface motion maps of Southern California," *IEEE Trans. Geosci. Remote Sens.*, vol. 45, no. 2, pp. 512–521, Feb. 2007.

[25] J. Hu *et al.*, "Vertical and horizontal displacements of Los Angeles from InSAR and GPS time series analysis: Resolving tectonic and anthropogenic motions," *J. Geodyn.*, vol. 99, pp. 27–38, Sep. 2016, doi: 10.1016/j.jog.2016.05.003.

[26] F. Guglielmino, G. Nunnari, G. Puglisi, and A. Spata, "Simultaneous and integrated strain tensor estimation from geodetic and satellite deformation measurements to obtain three-dimensional displacement maps," *IEEE Trans. Geosci. Remote Sens.*, vol. 49, no. 6, pp. 1815–1826, Jun. 2011.

[27] D. Massonnet, T. Holzer, and H. Vadon, "Land subsidence caused by the East Mesa geothermal field, California, observed using SAR interferometry," *Geophys. Res. Lett.*, vol. 24, no. 8, pp. 901–904, Apr. 1997.

[28] K. Mogi, "Relations between the eruptions of various volcanoes and the deformations of the ground surfaces around them," *Bull. Earthquake Res. Inst.*, vol. 36, pp. 99–134, Jul. 1958.

[29] D. W. Vasco, K. Karasaki, and L. Myer, "Monitoring of fluid injection and soil consolidation using surface tilt measurements," *J. Geotech. Geoenviron. Eng.*, vol. 124, no. 1, pp. 29–37, Jan. 1998.

[30] D. W. Vasco, L. R. John, and N. E. Goldstein, "Using surface displacement and strain observations to determine deformation at depth, with an application to Long Valley Caldera, California," *J. Geophys. Res.*, vol. 93, no. B4, pp. 3232–3242, Apr. 1988.

[31] D. W. Vasco, K. Karasaki, and C. Doughty, "Using surface deformation to image reservoir dynamics," *Geophysics*, vol. 65, no. 1, pp. 132–147, Jan. 2000.

[32] Z. Lu and W. R. Danskin, "InSAR analysis of natural recharge to define structure of a ground-water basin, San Bernardino, California," *Geophys. Res. Lett.*, vol. 28, no. 13, pp. 2661–2664, Jul. 2001.

[33] Z. Lu, T. Masterlark, and D. Dzurisin, "Interferometric synthetic aperture radar study of Okmok volcano, Alaska, 1992–2003: Magma supply dynamics and postemplacement lava flow deformation," *J. Geophys. Res.*, vol. 110, no. B2, pp. B02403-1–B02403-18, Feb. 2005.

[34] J. Hu, Q. J. Wang, Z. W. Li, R. Zhao, and Q. Sun, "Investigating the ground deformation and source model of the Yangbajing geothermal field in Tibet, China with the WLS InSAR technique," *Remote Sens.*, vol. 8, no. 3, p. 191, 2016.

[35] D. W. Vasco, C. Wicks, Jr., K. Karasaki, and O. Marques, "Geodetic imaging: Reservoir monitoring using satellite interferometry," *Geophys. J. Int.*, vol. 149, no. 3, pp. 555–571, Jun. 2002.

[36] D. W. Vasco, C. M. Puskas, R. B. Smith, and C. M. Meertens, "Crustal deformation and source models of the Yellowstone volcanic field from geodetic data," *J. Geophys. Res.*, vol. 112, no. B7, pp. B070402-1–B070402-19, Jul. 2007.

[37] I. Stakgold, *Green's Function and Boundary Value Problems*. Hoboken, NJ, USA: Wiley, 1979.

[38] Y. Okada, "Surface deformation due to shear and tensile faults in a half-space," *Bull. Seismol. Soc. Amer.*, vol. 75, no. 4, pp. 1135–1154, 1985.

[39] G. H. Golub and W. Kahan, "Calculating the singular values and pseudo-inverse of a matrix," *SIAM J. Numer. Anal.*, vol. 2, no. 2, pp. 205–224, 1965.

[40] C. C. Paige and M. A. Saunders, "LSQR: An algorithm for sparse linear equations and sparse least squares," *ACM Trans. Math. Softw.*, vol. 8, no. 1, pp. 43–71, Mar. 1982.

[41] C. Heliker and T. N. Mattox, "The first two decades of the Pu'u 'Ō'o-Kūpaianaha eruption: Chronology and selected bibliography," in *The Pu'u 'Ō'o-Kūpaianaha Eruption of Kilauea Volcano, Hawai'i: The First 20 Years*, C. Heliker, D. A. Swanson, and T. J. Takahashi, Eds. Washington, DC, USA: U.S. Geological Survey, 2003, pp. 1–28.

[42] M. Poland, A. Miklius, T. Orr, J. Sutton, C. Thornber, and D. Wilson, "New episodes of volcanism at Kilauea Volcano, Hawaii," *Eos Trans. Amer. Geophys. Union*, vol. 89, no. 5, pp. 37–38, Jan. 2008.

[43] M. Costantini, "A novel phase unwrapping method based on network programming," *IEEE Trans. Geosci. Remote Sens.*, vol. 36, no. 3, pp. 813–821, May 1998.

[44] Z. W. Li, X. L. Ding, D. W. Zheng, and C. Huang, "Least squares-based filter for remote sensingimage noise reduction," *IEEE Trans. Geosci. Remote Sens.*, vol. 46, no. 7, pp. 2044–2049, Jul. 2008.

[45] E. K. Montgomery-Brown *et al.*, "Geodetic evidence for en echelon dike emplacement and concurrent slow slip during the June 2007 intrusionand eruption at Kīlauea Volcano, Hawaii," *J. Geophys. Res.*, vol. 115, no. B7, pp. B07405-1–B07405-15, Jul. 2010.

[46] B. A. Brooks *et al.*, "Magmatically triggered slow slip at Kilauea Volcano, Hawaii," *Science*, vol. 321, p. 1177, Aug. 2008.
[47] H. S. Jung, J. S. Won, and S. W. Kim, "An improvement of the performance of multiple-aperture SAR interferometry (MAI)," *IEEE Trans. Geosci. Remote Sens.*, vol. 47, no. 8, pp. 2859–2869, Aug. 2009.
[48] J. Hu, X. L. Ding, Z. W. Li, J. J. Zhu, Q. Sun, and L. Zhang, "Kalman-filter-based approach for multisensor, multitrack, and multitemporal InSAR," *IEEE Trans. Geosci. Remote Sens.*, vol. 51, no. 7, pp. 4226–4239, Jul. 2013.

**Jun Hu** received the M.Eng. and Ph.D. degrees in geodesy and surveying engineering from Central South University, Changsha, China, in 2008 and 2013, respectively.

From 2013 to 2014, he was a Post-Doctoral Fellow with the Department of Land Surveying and Geo-Informatics, The Hong Kong Polytechnic University, Kowloon, Hong Kong. He is currently a Full Professor with the Department of Surveying and Remote Sensing, School of Geosciences and Info-Physics, Central South University. He has authored over 20 papers in international peer-reviewed journals. His current research interests include mapping 3-D surface displacement with interferometric satellite synthetic aperture radar technique and its applications in geophysical fields.

**Xiao-Li Ding** received the B.Eng. degree from the Central South University of Metallurgy, Changsha, China, in 1983, and the Ph.D. degree from The University of Sydney, Sydney, NSW, Australia, in 1993.

He was a Lecturer with the Northeast University of Technology, Shenyang, China, from 1983 to 1986, and with the Curtin University of Technology, Perth, WA, Australia, from 1992 to 1996. In 1996, he joined The Hong Kong Polytechnic University, Kowloon, Hong Kong, where he is currently with the Department of Land Surveying and Geo-Informatics as the Chair Professor of Geomatics. His current research interests include developing technologies for studying ground and structural deformation, geohazards, and spaceborne geodetic technologies, such as GPS and InSAR.

Dr. Ding is the President of Sub-Commission 4.4 of the International Association of Geodesy (IAG) on airborne and spaceborne imaging technologies. He is also a fellow of the IAG.

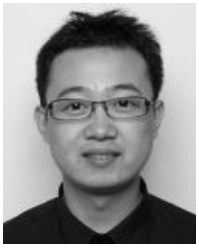

**Lei Zhang** (S'08–M'12) was born in Yantai, China, in 1981. He received the M.Eng. degree in geodesy and surveying engineering from Tongji University, Shanghai, China, in 2007, and the Ph.D. degree in geodesy and geodynamics from The Hong Kong Polytechnic University (HKPU), Kowloon, Hong Kong, in 2011.

He is currently a Research Assistant Professor with the Department of Land Surveying and Geo-Informatics, HKPU. His current research interests include developing advanced processing techniques for multiple SAR images and the application of multi-temporal SAR interferometric analysis to the retrieval of geophysical parameters and displacement monitoring, with emphasis on natural hazards.

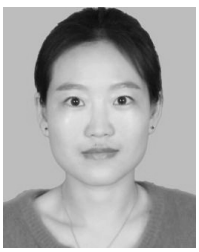

**Qian Sun** was born in Suqian, China, in 1983. She received the master's and Ph.D. degrees in geodesy and surveying engineering from Central South University, Changsha, China, in 2009 and 2015, respectively.

She is currenlty a Lecturer with the College of Resources and Enviromental Science, Hunan Normal University, Changsha. Her current research interests include monitoring geo-hazards with multi-temporal interferometric satellite synthetic aperture radar techniques.

**Zhi-Wei Li** received the bachelor's and master's degree in surveying engineering from the Central South University of Technology (currently Central South University), Changsha, China, in 1997 and 1999, respectively, and the Ph.D. degree in remote sensing from The Hong Kong Polytechnic University, Kowloon, Hong Kong, in 2005.

He is currently a Full Professor with the Department of Surveying and Remote Sensing, School of Geosciences and Info-Physics, Central South University. He has authored over 50 papers in international peer-reviewed journals. His current research interests include interferometric synthetic aperture radar for mining, permafrost, and glacier motion monitoring, particularly their 3-D deformation mapping.

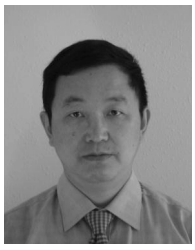

**Jian-Jun Zhu** received the M.Eng. degree in engineering surveying and the Ph.D. degree in geodesy and surveying engineering from the Central South University of Technology (now Central South University), Changsha, China, in 1985 and 1998, respectively.

From 1998 to 1999, he was a Research Assistant with the Department of Land Surveying and Geo-Informatics, The Hong Kong Polytechnic University, Hong Kong. From 2000 to 2001, he was a Post-Doctoral Fellow with the Center for Research on Geomatics, Laval University, QC, Canada. He is currently a Full Professor with the School of Geosciences and Info-Physics, Central South University. His current research interests include the theory of errors and surveying adjustment and its applications in interferometric satellite synthetic aperture radar and global positioning systems.

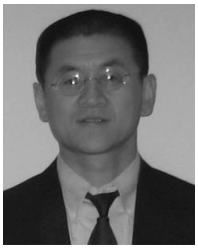

**Zhong Lu** (S'96–A'97–M'97–SM'07) received the B.S. and M.S. degrees from Peking University, Beijing, China, in 1989 and 1992, respectively, and the Ph.D. degree from the University of Alaska Fairbanks, Fairbanks, QC, Canada, in 1996.

He was a Physical Scientist with the United States Geological Survey, Reston, VA, USA, from 1997 to 2013. He is currently a Professor and Endowed Shuler-Foscue Chair with the Huffington Department of Earth Sciences, Southern Methodist University, Dallas, TX, USA. He is also a Principal Investigator of Projects funded by NASA, ESA, JAXA, DLR, and the USGS on the study of land surface deformation using satellite InSAR imagery. He has published over 45 lead-authored and 90 co-authored peer-reviewed journal articles and book chapters, which focused on InSAR techniques and applications. He has authored the book titled *InSAR Imaging of Aleutian Volcanoes: Monitoring a Volcanic Arc from Space* (Springer, 2014). His current research interests include technique developments of SAR, InSAR, and persistent scatterer InSAR processing and their applications on natural hazard monitoring and natural resource characterization.

Dr. Lu is a Committee Member of the International User Team for Radarsat-C SAR Constellations, the GeoEarthscope InSAR User Working Group, the NASA's Alaska Satellite Facility User Working Group, and the upcoming NASA-India SAR Science Definition Team. He was a recipient of the American Society for Photogrammetry and Remote Sensing Award for Best Scientific Paper in Remote Sensing, the NASA Group Achievement Award, the NASA Certificate of Appreciation, the Raytheon Distinguished Level Award for Excellence in Technology, the Science Applications International Corporation Technical Fellowship, and the Jerald Cook Memorial Award. He is the Chair of Western North America InSAR Consortium. He is an Associate Editor of Remote Sensing and Frontier in Volcanology, and a member of editorial boards of the International Journal of Image and Data Fusion, Geomatics, Natural Hazards and Risk, and Dataset Papers in Geosciences.